

Cluster Catch Digraphs with the Nearest Neighbor Distance

Rui Shi, Elvan Ceyhan, and Nedret Billor

Department of Mathematics and Statistics

Auburn University

November 12, 2025

Abstract

We introduce a new clustering method based on Cluster Catch Digraphs (CCDs). The new method addresses the limitations of RK-CCDs on clustering by employing a new variant of spatial randomness test that employs the nearest neighbor distance (NND) instead of the Ripley's K function. Our method is particularly effective for high-dimensional datasets, comparable to or outperforming KS-CCDs and RK-CCDs (rely on a KS-type statistic or the Ripley's K function) on clustering. We conduct a comprehensive Monte Carlo analysis to assess the performance of our method, considering factors such as dimensionality, dataset size, number of clusters, cluster volumes, and inter-cluster distance. We also evaluate our methods using real and complex datasets, comparing them to well-known clustering methods. Again, our methods exhibit competitive performance, producing high-quality clusters with desirable properties.

Keywords: Graph-based clustering; Cluster catch digraphs; High-dimensional data; the nearest neighbor distance; Spatial randomness test.

1 Introduction and Motivation

Clustering is a fundamental Statistical method for partitioning observations into groups based on similarity or proximity. It is an unsupervised learning method that plays a crucial role in machine learning and pattern recognition. The primary goal is to group a dataset so that points in the same group (called a cluster) are similar. Clustering faces challenges like determining the optimal number of clusters and handling high-dimensional data. Driver and Kroeber first introduced cluster analysis in 1932 [16],

applying it to anthropology. Early clustering methods focused on k -means and hierarchical methods, which are the fundamentals of cluster analysis [58, 37]. Since then, clustering methods have evolved substantially and are widely used across various disciplines. Common examples include partitioning customers into distinct groups for better market strategy [66], grouping genes that have a similar physiological expression in biology [19], enhancing image processing by dividing and re-grouping [13], and predicting human behavior based on their communities and social ties [26]. Despite significant advancements, clustering still remains challenging, due to the fact including determining the optimal number of clusters [41], scalability to large datasets [74], robustness to outliers and noise [53], and handling high-dimensional data [6].

In our previous work, We have proposed a graph- and distribution-based clustering method, called UN-CCDs [56], aiming to overcome the limitations of its two predecessors: KS-CCDs and RK-CCDs. Specifically, RK-CCDs are ineffective for high-dimensional clustering due to Ripley’s K function in MC-SRT; and KS-CCDs are not parameter-free, an intensity parameter δ is needed for a KS-type statistic. We first recap the CCD-based method below.

Cluster Catch Digraphs (CCDs) are a family of graph-based clustering methods, which were first introduced by DeVinney [14] and Marchette [40], adapted from a similar classification digraph called **Class Cover Catch Digraphs** (CCCDs). Later, Manukyan and Ceyhan [39] advanced this approach further, developing two variants using a Kolmogorov-Smirnov (KS)-type statistic and Ripley’s K function, calling them KS-CCDs and RK-CCDs, respectively. RK-CCDs and KS-CCDs work similarly on clustering. While both are effective, RK-CCDs are particularly appealing for being “almost” parameter-free, unlike KS-CCDs, which require an input intensity parameter for the KS-type statistic.

However, despite their advantages, RK-CCDs are not suitable for clustering moderate to high-dimensional data, as shown by our intensive simulation study [56]. This gap motivates the need for a new CCD-based clustering method that is robust in higher dimensions, while remaining parameter-free.

To address this challenge, we had made the following contribution in this paper:

- (i) We proposed a new clustering method called UN-CCDs (Uniformity- and Neighbor-based CCDs), which is “almost” parameter-free.
- (ii) UN-CCDs address the limitations of RK-CCDs by using the nearest neighbor distance (NND) for a spatial randomness test instead of the Ripley’s K function,

Making this method more effective for high-dimensional datasets.

- (iii) By extensive Monte Carlo analysis, We show that UN-CCDs are competitive with or superior to other well-known traditional or recent clustering methods.
- (iv) The UN-CCD method can provide high clustering quality under different levels of noise.

The article is organized as follows: (1) In Section 2, we review the state-of-the-art clustering methods from different categories, plus the mathematical foundation of KS-CCDs and RK-CCDs. (2) Section 3 details the limitations of RK-CCDs first, followed by the motivation and the algorithmic formulation of UN-CCDs. (3) In Section 4 and 5, we apply UN-CCDs to real and complex datasets, demonstrating its advantages over RK-CCDs, KS-CCDs, and traditional clustering methods such as DBSCAN, *K*-means++, etc.

2 Preliminaries

2.1 Cluster Methods in Literature

In literature, cluster-based methods have been classified into several subgroups, known as partitional, hierarchical, density-based, grid-based, fuzzy-based, model-based, and distribution-based clustering methods. We provide a short summary of these method below. [63, 69, 21].

Partitioning clustering methods iteratively partition data into a predefined number (k) of clusters, often minimizing within-cluster distances [63, 69]. They are generally efficient but require k as input and are sensitive to outliers [69]. Classic examples include ***K*-Means** [25], ***K*-Means++** [3], **MacQueen** [37]. **PAM** [35] is more robust to outliers, but computationally expensive [69]. More recent methods, such as **CLARA** [35] and **CLARANS** [43], address the computational cost of PAM on large datasets.

Hierarchical clustering methods construct a dendrogram with agglomerative (bottom-up) or divisive (top-down) methods, without the need to pre-define the number of clusters. Those methods offer interpretability but can be computationally costly for large datasets [47]. Classic examples include the **Ward’s minimum variance method** [65] and **minimal spanning tree** [70], but they are computationally intensive and struggle with arbitrarily-shaped clusters [72]. More recent methods, such as **CURE** [27], **CHAMELEON** [34], and **ROCK** [28] aim to overcome these limitations.

Density-based clustering methods identify clusters as high-density regions, separating them by low-density areas. They typically do not require k as an input parameter, capable to find arbitrarily shaped clusters, and are robust to outliers [20]. A typical classic example is **DBSCAN** [20], but its performance is sensitive to the values of two input parameters (**Eps** and **MinPts**), and has limitations on clusters with varying intensities. Later methods were developed to solve one or two disadvantages of DBSCAN, including **OPTICS** [2], **DBCLASD** [68], and **DENCLUE** [29].

Graph-based clustering methods partition nodes (points) by leveraging a graph's connectivity structure, aiming to identify sub-graphs for latent clusters. A key advantage of those methods is their ability to identify non-convex clusters where vector-based approaches may fail [52]. Well-known classic examples include the **Minimal Spanning Tree** (MST) [70], **spectral clustering** [42], but these methods are either sensitive to outliers or computationally intensive. More recent and scalable methods include **Louvain** [8] and **Leiden** [60], which are designed for large datasets. We also have deep learning methods like **Structural Deep Clustering Network (SDCN)** [9]. This paper focuses on CCD-based methods, specifically RK-CCDs and KS-CCDs [39], which will be discussed in detail shortly. In Section 5, we will use real-life datasets to compare UN-CCDs with some commonly used graph-based methods, including MST, spectral clustering, and Louvain. We will discuss the mechanisms and setup of those methods in Section 5.

Recent work in graph clustering has focused on tackling the challenges of high-dimensional data and developing more robust methods. The “curse of dimensionality” poses a significant challenge for traditional clustering algorithms, as distances between any pairs of points become meaningless in high-dimensional spaces. UN-CCDs address this by employing a spatial randomness test with several key enhancements compared to the one employed in RK-CCDs, making it more robust to high-dimensional data. Recent research in this area also focuses on high-dimensional data and using robust statistics to identify and handle outliers that can negatively impact performance. Methods like **RSC-SGM** (Robust Spectral Clustering for Sub-Gaussian Mixtures) construct a Gaussian-kernel similarity graph, apply a denoising step to the affinity matrix, and use a rounding procedure to achieve accurate and automatic clustering and outlier detection [59]. **NA-COV** (Network-Adjusted Covariates) integrates high-dimensional node covariates with network structure to improve community detection in sparse graphs [31]. **BayesCov-SBM** (Bayesian Community Detection with Covariates) uses a joint model

called Bayesian stochastic block model that incorporates both network structure and high-dimensional node covariates for community detection [55].

Graph-based clustering methods, including the CCD-based framework, Leverage the digraph’s connectivity and relative distance for clustering. A key advantage of CCD-based methods is identifying non-convex clusters [39], where vector-based approaches like *K*-Means and Hierarchical clustering may fail. Additionally, unlike density-based methods like DBSCAN that identify the “seeds” of clusters in high-density regions exceeding a density threshold, most CCDs do not require the user to define such a threshold. Instead, CCDs create a digraph where arcs are determined by a spatial randomness test for each data point, effectively identifying local clusters. CCD-based methods also differ from modularity-based graph methods, such as Louvain, which partitions a network by maximizing a measure of community structure. While Louvain and other similar methods are designed for large networks, CCDs are particularly focused on using geometric properties of the data itself to define the graph structure and clusters.

Several modern categories of clustering, including grid-based, model-based, and fuzzy-based clustering methods were developed to address specific challenges like large-scale data, statistical rigor, and ambiguous cluster boundaries.

Grid-based clustering methods partition the data space into a grid structure and perform clustering on the grid cells. Their time/space complexity depends on grid size rather than data size, making them fast for large datasets [64]. The clustering quality relies on grid granularity, and they may struggle with irregular cluster boundaries [69]. Examples include **STING** [64], **WaveCluster** [54], **DClust** [73], and **CLIQUE** [1].

Model-based clustering methods assume data originates from a mixture of probability distributions, these methods fit models to identify clusters [47]. They offer flexibility in cluster shape/size and support “soft” assignments but can be computationally intensive and are sensitive to model/parameter choices [69]. Examples include **GMMs** [48], **LDA** [7], **HMM** [46], **COBWEB** [22], **pdfCluster** [4], and **SOM** [62].

Fuzzy Clustering is known as “soft” clustering, these methods allow data points to belong to multiple clusters with varying degrees of membership [21], useful for ambiguous or overlapping boundaries [35]. Optimization can be computationally intensive [21]. Examples include **Fuzzy C-means** (FCM) [18], which is sensitive to initialization and outliers [52]; the more robust **Possibilistic-fuzzy C-means** (PFCM) [44, 36]; and **Kernelized Fuzzy C-means** (KFCM) for non-linear boundaries [71].

2.2 Cluster Catch Digraphs

Our clustering methods are based on Cluster Catch Digraphs (CCDs), where vertices represent the points of a given dataset X , and arcs are determined by the spherical ball (covering ball) centered at each point. Class Cover Catch Digraphs (CCCDs) [45] are the prototypes of CCDs, originally designed for supervised classification. CCCDs aim to distinguish a target class from a non-target class by covering the target class points with a minimum number of balls while excluding the non-target points [40]. A CCCD is constructed by creating covering balls around each point, forming arcs between points when one lies within the covering ball of another. Two variants, pure-CCCDs (P-CCCDs) and random walk-CCCDs (RW-CCCDs), differ in how the radius of each covering ball is determined [38]. CCDs are an unsupervised adaptation of CCCDs [40], initializing by constructing a covering ball for each point. To reduce the covering complexity in CCDs and avoid overfitting, we retain only a subset of covering balls that optimally covers all (or most) points in a dataset. One way is finding a **minimum dominating set** (MDS) of the CCD. Although finding the MDS of a digraph is an NP-Hard problem [33], one can find an approximation of MDS efficiently with the Greedy Algorithm, which operates in $O(|V_0|^2)$ time [10, 30]. The Greedy Algorithm finds an approximate MDS by iteratively selecting the vertex with the highest outdegree at each iteration and storing this point in a set, and removing its closed neighborhood (in the graph) from the uncovered vertices until all vertices are covered. When the algorithm terminates, the stored vertices are retained for the (approximate) MDS. Manukyan and Ceyhan proposed two variants of the Greedy Algorithm for CCDs [39]: the first variant prioritizes vertices closer to cluster centers, while the second maximizes a score function at each step. We provide these methods in Algorithms 1 and 2, respectively for completeness, because they are non-standard in their greediness and also for future reference.

2.2.1 Cluster Catch Digraphs Based on a KS-Type Statistic

CCDs, introduced by Devinney [14], are an adaptation of CCCDs [45] for unsupervised clustering. Given an unlabeled dataset $X = \{x_1, x_2, \dots, x_n\} \subset \mathbb{R}^d$, where points are drawn from a mixture distribution, the objective is to determine the number of clusters and the optimal data partitioning. Unlike CCCDs, CCDs determine the radius of each covering ball $B(x_i, r_{x_i})$ (centered at x_i with radius r_{x_i}) using a Kolmogorov-Smirnov (KS)-type statistic, which measures the deviation of the local intensity around each

Greedy Algorithm 1: A greedy algorithm to find an approximate MDS of CCDs (which **does not** update the digraph after each iteration). V and A are the initial vertex and edge sets of the digraph D , respectively. $\bar{N}(v)$ is the closed neighborhood of a vertex v (i.e., the points covered by the covering ball centered at v , including v itself). At each iteration, V_{temp} represents the uncovered vertices, and v_{temp} is the vertex with largest outdegree.

Input: A digraph $D = (V(D), A(D))$ where $X = \{x_1, x_2, \dots, x_n\}$

Output: A approximate minimum dominate set \hat{S}

```

1 Initialization:  $V_{temp} \leftarrow V(D)$ ,  $\hat{S} \leftarrow \emptyset$ 
2 while  $V_{temp} \neq \emptyset$  do
3    $v_{temp} \leftarrow \arg \max_{v \in V \setminus \hat{S}} \{d_{out}^*(v)\}$ ;      ( $d_{out}^*(v)$ : the outdegree of  $v$  in  $D$ )
4    $V_{temp} \leftarrow V_{temp} \setminus \bar{N}(v_{temp})$ ;
5    $\hat{S} \leftarrow \hat{S} \cup \{v_{temp}\}$ ;
end

```

Greedy Algorithm 2: A greedy algorithm to find an approximate MDS which is greedy in a score function $sc(v)$ at each iteration (digraph is updated after each iteration). $D_{sub}(S)$ is the induced sub-digraph of vertex set S from a digraph D .

Input: A digraph $D = (V(D), A(D))$. for a given dataset $X = \{x_1, x_2, \dots, x_n\}$

Output: A approximate minimum dominate set \hat{S} .

```

1 Initialization:  $V_{temp} \leftarrow V(D)$ ,  $\hat{S} \leftarrow \emptyset$ 
2 while  $V_{temp} \neq \emptyset$  do
3    $v_{temp} \leftarrow \arg \max_{v \in V(D)} \{sc(v)\}$ ;      ( $sc(v)$ : the score function for  $v$ )
4    $V_{temp} \leftarrow V_{temp} \setminus \bar{N}(v_{temp})$ ;
5    $\hat{S} \leftarrow \hat{S} \cup \{v_{temp}\}$ ;
6    $D \leftarrow D_{sub}(V_{temp})$ ;
end

```

point x_i from a null model such as the **Complete Spatial Randomness** (CSR, where points are distributed uniformly within a given area) [40], the KS-type statistic for a point x_i is defined as:

$$T_{KS}(x_i, r) = F_{RW}(x_i, r) - F_0(x_i, r), \quad (1)$$

where $F_{RW}(x_i, r)$ represents the number of points within the covering ball $B(x_i, r)$, and $F_0(x_i, r)$ is the expected number of points under the null model, typically given by $F_0(x_i, r) = \delta r^d$ under the assumption of CSR, where δ is a density parameter and d is the dimension of the space.

The radius r_{x_i} of a covering ball $B(x_i, r_{x_i})$ is chosen to maximize its KS-type statistic:

$$r_{x_i} = \arg \max_{r \geq 0} \{T_{KS}(x_i, r)\}, \quad (2)$$

which ensures that the points covered by $B(x_i, r_{x_i})$ (including x_i) form a significant local cluster.

Once the optimal radii are determined for all covering balls, a digraph for X is constructed, denoted as $D = (V(D), A(D))$, where $V(D) = X$, and there is an arc from x_i to x_j ($x_i x_j \in A(D)$) if $x_j \in B(x_i, r_{x_i})$. Once the digraph D is constructed, the weakly connected components of D can be taken as clusters.

In order to prevent the impact of noise, one may want to reduce the “complexity” of the covering balls. To achieve this goal, we apply the Greedy Algorithm 1 to find an approximate MDS, denoted as \hat{S} , which selects a subset of covering balls, representing the clusters more efficiently [40]. The algorithm iteratively selects the vertex with the largest outdegree (i.e., the vertex with covering ball covering the most points) until all points are covered.

To further reduce the complexity of the cluster cover, an **intersection graph** $G_{MD} = (V_{MD}, E_{MD})$ is constructed, where $V_{MD} = \hat{S}$, and an edge exists between $u, v \in \hat{S}$ if their covering balls cover some common points, i.e., $\bar{N}(u) \cap \bar{N}(v) \neq \emptyset$. The Greedy Algorithm 2 is then applied to G_{MD} to prune the MDS \hat{S} further, yielding a reduced set $\hat{S}(G_{MD})$ that represents the center of latent clusters, and an initial partition $P = \{P_1, P_2, \dots, P_k\}$ for X can be constructed based on $\hat{S}(G_{MD})$.

Finally, to remove noise or outlying clusters, Manukyan and Ceyhan [39] designed an automatic refinement process based on **silhouette index** (a metric measures the quality of clustering) [24]. This process first ranks the partitions in P in a decreasing order based on their size. Starting from the first two, it adds partitions incrementally as valid clusters until the average silhouette index of the entire dataset is maximized, indicating the optimal number of clusters is reached. In summary, the refinement process works on a set of candidate partitions (or clusters) and the final, selected ones are the finalized clusters, whose covering balls are the **dominating covering balls**.

During the above automatic refinement process, re-partitioning occurs after each incremental addition of a new partition, in order to re-evaluate the overall average silhouette index. In the re-partitioning step, points are assigned to the existing partition with the smallest relative dissimilarity measure $\rho(x_i, B(x_j, r_{x_j}))$, which is defined as

follows,

$$\rho(x_i, B(x_j, r_{x_j})) = \frac{d(x_i, x_j)}{r_{x_j}}, \quad (3)$$

where $d(x_i, x_j)$ is any distance or dissimilarity measure and $B(x_j, r_{x_j})$ is the covering ball for a existing partition during this process.

2.2.2 Cluster Catch Digraphs Based on Ripley's K Function

Although the KS-CCD method is robust to noise clusters thanks to the employment of the silhouette index, it still has some limitations. For example, the KS-CCD method is not able to capture the spatial distributions of each cluster, and it need an input density parameter δ to determine the radius of each covering ball [39]. To address those limitations, instead of using the KS-type statistic, Manukyan and Ceyhan [39] applied the Ripley's K function [50], denoted as $K(t)$, to construct a test determining whether the points within each covering ball follow a **homogeneous Poisson process** (HPP, i.e., Complete Spatial Randomness). This test is referred to as the **Spatial Randomness Monte Carlo Test** (MC-SRT) with Ripley's K function.

More specifically, given a dataset X consists of *i.i.d* points $\{x_1, x_2, \dots, x_n\}$ in a region $R \subset \mathbb{R}^d$, the Ripley's K function measures the spatial distribution of X , revealing whether the points of X are clustered, dispersed, or randomly distributed. It is defined as follows [15],

$$K(t) = \lambda^{-1} E[\text{the number of additional pairs of points within distance } t], \quad (4)$$

where λ is the density of the point set.

K function can be applied to describe certain point patterns of X and the most common application is to test CSR [15], where the test statistic is the estimator of $K(t)$, denoted as $\hat{K}(t)$, which is proportional to the ratio of the actual number of pairs whose distance is less than t against the intensity of the point set. For more details, please refer to Manukyan and Ceyhan's work [39].

The RK-CCD method sets the radius of each covering ball to the largest value for which the points inside the ball fail to reject the null hypothesis of CSR, ensuring that the points encapsulated conform to a CSR pattern. The primary difference between RK-CCDs and KS-CCDs is in the determination of the radii, which is now based on Ripley's K function rather than the KS-type statistic. Subsequent steps, such as reducing cover complexity using an approximate MDS, and refining the clustering result by maximizing

the silhouette index, remains the same as in KS-CCDs.

A variant of RK-CCDs introduced by Manukyan and Ceyhan allows for the detection of clusters with arbitrary shapes by considering the connected components of the intersection graph G_{MD} as the final clusters instead of using the MDS [39].

3 Cluster Catch Digraphs using the Nearest Neighbor Distance

3.1 The Limitations of RK-CCDs for Clustering

In our previous work,, we proposed the U-MCCD and SU-MCCD methods for outlier detection [56], where SU-MCCDs are the “flexible” versions of U-MCCD, adaptable for arbitrarily shaped clusters. As their first step, both methods employ RK-CCDs for clustering. However, the Monte Carlo analysis reveals that outlier detection with U-MCCDs and SU-MCCDs exhibit high **False Positive Rates** (TNRs) for regular points (falsely identifying regular points as outliers) in high-dimensional datasets. We have shown that this degradation is attributed to the limitations of RK-CCDs in high-dimensional spaces, whose dominating covering balls are not sufficiently large for latent clusters [56].

Specifically, RK-CCDs present two key limitations [56]: (1) The initial points in the MC-SRT are not random, as they are always the centers of the covering balls, leading to inaccurate testing results, especially in high-dimensional datasets; (2) In MC-SRT, the point-wise confidence band for $K(t)$ is constructed on fixed t values [39], which is not appropriate when the dimensions are not fixed, especially for high-dimensional datasets, where the distances between any two points get arbitrarily large.

3.2 The MC-SRT with the Nearest Neighbor Distance

To avoid the limitations of RK-CCDs, we have introduced a new CCD approach for several new outlier detection methods and scores [56, 57]. This new CCD conduct MC-SRT with the **Nearest Neighbor Distance** (NND) instead of the Ripley’s K function.

Given a dataset $X = \{x_1, x_2, \dots, x_n\}$, the mean NND of X is $\bar{d} = \frac{\sum_{i=0}^n d_i}{n}$, where d_i represents the distance of x_i to its nearest neighbor. We aim to compares \bar{d} with the expected mean NND (denoted as μ_d) under the assumption of CSR. A normality test offers a convenient way to obtain p -values for \bar{d} . Because both μ_d and $\sigma_{\bar{d}}$ (the standard derivation of \bar{d} under the assumption of CSR) can be derived [11, 12]. However, when

the sample size n is small, the distribution of \bar{d} is skewed, making the normality test unfeasible [5]. Fortunately, a Monte Carlo test proposed by Besag and Diggle [5] provides an alternative, where the p -values are determined by the empirical quantiles.

Consequently, we have proposed another CCD approach based on the MC-SRT with NND. Specifically, we made several key enhancements to boost the robustness and reliability of the new CCDs [56]: (1) We conduct MC-SRT with both median and mean NND, applying a Holm’s Step-Down Procedure for correction [67], which improves the accuracy of the test substantially; (2) Our previous work shows that larger covering balls for each point are preferred for high-dimensional datasets [56]. Therefore, we offer the option to test the candidate radius values in a descending order, stops when the current radius value is not rejected in MC-SRT. (3) The MC-SRT is lower-tailed as the upper tail indicates the point pattern is significantly “regular”, which is less relevant to our interest. (4) The center points are excluded from the test as they are not random.

The new clustering approach based on CCDs and NND is called **Uniformity- and Neighbor-based CCD** (UN-CCD) clustering method, which is presented in Algorithm 8. It is worth noting that the only difference among KS-CCDs, RK-CCDs, and UN-CCDs is how to determine the radius of covering balls. The time and space complexities of UN-CCDs for clustering are $O((N + d)n^2 + n^3)$ and $O(n^2)$ respectively, which we have proven in our previous work [56].

We summarize the time and space complexity of RK-CCDs, KS-CCDs, and UN-CCDs in Table 1. When N and d are fixed, KS-CCDs and UN-CCDs have the time complexity of $O(n^3)$, while RK-CCDs run in $O(n^3 \log n)$, slower than the other two. All the three methods have the same space complexity of $O(n^2)$.

The clustering procedure with UN-CCDs for a 2-dimensional dataset consisting of 5 clusters is illustrated in Figure 1.

In Section 4, we compare the performance of KS-CCDs, RK-CCDs, and UN-CCDs with synthetic datasets consisting of multiple clusters. We show the advantage of UN-CCDs over RK-CCDs on Gaussian clusters and in high-dimensional settings.

Algorithm 8: (UN-CCD Clustering method) Cluster Catch Digraphs based on the Nearest Neighbor Distance (NND). α is the level of the Monte Carlo test with NND.

Input: α , dataset $X = \{x_1, x_2, \dots, x_n\}$;
Output: Cluster centers of X ;

Algorithm Steps:

```

1 foreach  $x_i \in X$  do
2   Calculate distances  $D(x_i) = \{d(x_i, x_j) | x_j \in X, x_i \neq x_j\}$ ;
3   foreach distance  $r_{(j)}$  in  $D(x_i)$  sorted ascending do
4     Perform the MC-SRT with NND on the  $X \cap B(x_i, r_{(j)})$ ;
5     if test rejected at level  $\alpha$  then
6       Set  $r_{x_i} = r_{(j-1)}$ ; break;
7     end
8   end
9 end
10 Construct a CCD,  $D = (V, A)$  using the pre-determined radii;
11 Find the approximate minimum dominating set  $\hat{S}(V)$  in  $D$  with the Greedy
    Algorithm 1;
12 Create intersection graph  $G_{MD} = (V_{MD}, E_{MD})$  with  $\hat{S}(V)$ ;
13 Find an approximate minimum dominating set  $\hat{S}(G_{MD})$  in  $G_{MD}$  using the
    Greedy Algorithm 2 with a score function measuring the number of points
    covered, stops when the average silhouette index  $Sil(P)$  is maximized;
14 Output  $\hat{S}(G_{MD})$  as cluster centers;

```

Algorithms	Time Complexity	Space Complexity
KS-CCDs	$O(n^3 + n^2(d + \log n))$	$O(n^2)$
RK-CCDs	$O(n^3(\log n + N) + n^2d)$	$O(n^2)$
UN-CCDs	$O((N + d)n^2 + n^3)$	$O(n^2)$

Table 1: The time/space complexity of all CCD-based methods.

4 Monte Carlo Experiments for Clustering Based on UN-CCDs

4.1 Experiment with Uniform Settings

This section presents a Monte Carlo analysis of CCD-based clustering using synthetic datasets. These datasets are generated with varying dimensionality d , dataset size n , number of clusters, and cluster volumes.

Similar to the design of simulations in our previous work [56], the analysis begins with datasets consisting of uniform clusters.

The varied simulation factors are enumerated as follows:

- i. Dimensionality (d): 2, 3, 5, 10, 20;

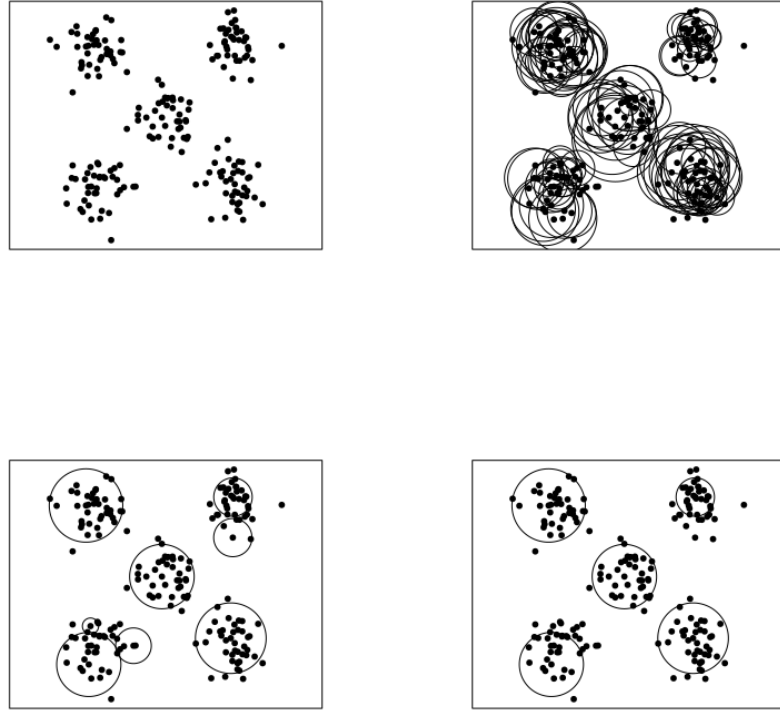


Figure 1: A illustration of clustering with UN-CCDs. **Top-left:** A dataset consisting of 5 clusters generated from 5 different bivariate normal distributions. **Top-right:** The covering balls of an approximate MDS obtained by Greedy Algorithm 1. **Bottom-left:** The covering balls of an approximate MDS of the intersection graph. **Bottom-right:** The dominating covering balls of the intersection graph that maximize silhouette index $Sil(P)$.

ii. Dataset size (n): 50, 100, 200, 500;

iii. Number of clusters (# clusters): 2, 3, 5.

Additionally, all simulated datasets share the following common factors:

- Cluster radii is a random variable between 0.8 and 1.2 (uniformly distributed);
- Equal cluster sizes (with varying support volumes and intensities due to the changing radii);

Additionally, the cluster centers are:

- 1st cluster: $\mu_1 = (\underbrace{3, \dots, 3}_d);$
- 2nd cluster: $\mu_2 = (6, \underbrace{3, \dots, 3}_{d-1});$
- 3rd cluster: $\mu_3 = (6, 6, \underbrace{3, \dots, 3}_{d-2});$

- 4th cluster: $\mu_4 = (3, 5.5, \underbrace{3, \dots, 3}_{d-2})$;
- 5th cluster: $\mu_5 = (8.5, \underbrace{3, \dots, 3}_{d-1})$.

The minimal distances between the first three cluster centers are 3, ensuring well separate clusters. On the other hand, the distances between the 1st and the 4th, the 2nd and the 5th cluster centers are 2.5, leading in closer clusters, which may be confused as one cluster by many clustering methods. This study investigates the performance of the three CCD-based clustering methods for close clusters. We present three realizations with different number of clusters under 2-dimensional space in Figure 2.

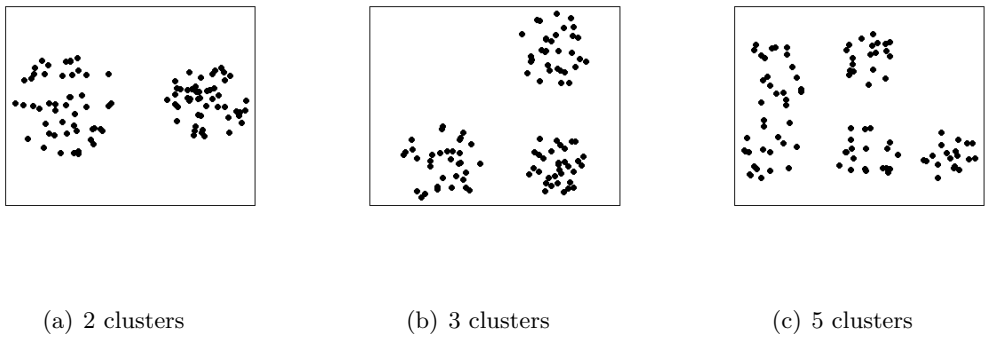


Figure 2: Realizations of the simulation settings with 2, 3, and 5 uniform clusters in \mathbb{R}^2 .

Clustering quality is assessed using both internal and external validation measures, including the Adjusted Rand Index (**ARI**) [32], the average silhouette index (**Sil**) [51], and the frequency of successfully identifying the corrected number of clusters (denoted as success rate or **SR** for simplicity). We repeat each simulation 500 times, and the average measures across these repetitions are recorded.

To accommodate the decreased data intensity in high-dimensional datasets, one may increase the volumes of covering balls as dimensions increase. A smaller significance level α of MC-SRT (for both RK-CCDs and UN-CCDs) leads to larger radius for the covering balls. Therefore, we can achieve this objective by tuning the significance level α of MC-SRT (for both RK-CCDs and UN-CCDs). After some trial-and-error process (not shown here), we set α to 1% for $d < 10$ and 0.1% for $d \geq 10$ for RK-CCDs, which achieves the best overall performance. For UN-CCDs, the α of the MC-SRT (with NND) is set to $\{15\%, 10\%, 5\%, 1\%, 0.1\%\}$ as d increases from 2 to 20 for the optimal performance. Unlike RK-CCDs and UN-CCDs, KS-CCDs require a density parameter δ for the KS-type statistic. To manage the scale of δ in high-dimensional settings, We work on the value of $\sqrt[d]{\delta}$ instead, and select the $\sqrt[d]{\delta}$ maximizing the average silhouette index in each

simulation, presented in Tables 2 and 6. The simulation results are summarized in Tables 3, 4, and 5. For better visualization, we summarize the simulation results in the following line plots (Figures 3 to 5), illustrating the trend of the performance (ARIs) of each CCD-based methods with varying data sizes (n), dimensions (d), and the number of clusters. To keep the figures uncluttered, we fix the number of clusters to 3 for the line plots with varying data sizes and dimensions; and the data size n is fixed to 200 when we study the performance trend as the number of clusters increases.

Density Parameter: $\sqrt[d]{\delta}$		$d = 2$	$d = 3$	$d = 5$	$d = 10$	$d = 20$
$n = 50$	2 clusters	3.70	2.00	1.30	0.75	0.49
	3 clusters	3.10	1.80	1.20	0.700	0.55
	5 clusters	2.60	1.60	1.10	0.800	0.69
$n = 100$	2 clusters	5.20	2.50	1.50	0.80	0.53
	3 clusters	4.40	2.40	1.30	0.78	0.56
	5 clusters	3.80	2.10	1.30	0.88	0.70
$n = 200$	2 clusters	7.00	3.00	1.50	0.85	0.60
	3 clusters	5.90	3.10	1.50	0.82	0.57
	5 clusters	5.40	2.70	1.50	0.98	0.74
$n = 500$	2 clusters	11.00	3.90	1.70	0.88	0.62
	3 clusters	9.00	3.50	1.90	0.85	0.60
	5 clusters	8.40	3.70	1.90	1.10	0.72

Table 2: The optimal scaled densities ($\sqrt[d]{\delta}$) of KS-CCDs on synthetic datasets consisting of uniform clusters.

KS-CCDs		$d = 2$			$d = 3$			$d = 5$			$d = 10$			$d = 20$		
		ARI	Sil	SR	ARI	Sil	SR	ARI	Sil	SR	ARI	Sil	SR	ARI	Sil	SR
$n = 50$	2 clusters	0.997	0.698	0.998	0.999	0.665	1.000	0.999	0.632	1.000	1.000	0.608	1.000	1.000	0.594	1.000
	3 clusters	0.984	0.680	0.964	0.996	0.654	0.998	0.999	0.627	1.000	1.000	0.600	1.000	1.000	0.584	1.000
	5 clusters	0.879	0.603	0.622	0.922	0.584	0.772	0.972	0.565	0.922	0.998	0.546	0.998	1.000	0.536	1.000
$n = 100$	2 clusters	1.000	0.698	1.000	1.000	0.665	1.000	1.000	0.634	1.000	1.000	0.606	1.000	1.000	0.591	1.000
	3 clusters	0.999	0.687	0.998	0.999	0.654	1.000	1.000	0.625	1.000	1.000	0.598	1.000	1.000	0.585	1.000
	5 clusters	0.952	0.619	0.860	0.962	0.590	0.900	0.989	0.567	0.976	0.999	0.547	1.000	1.000	0.535	1.000
$n = 200$	2 clusters	1.000	0.698	1.000	1.000	0.666	1.000	1.000	0.631	1.000	1.000	0.606	1.000	1.000	0.589	1.000
	3 clusters	1.000	0.688	1.000	1.000	0.655	1.000	1.000	0.626	1.000	1.000	0.600	1.000	1.000	0.587	1.000
	5 clusters	0.983	0.625	0.966	0.990	0.596	0.980	0.996	0.570	1.000	1.000	0.548	1.000	1.000	0.535	1.000
$n = 500$	2 clusters	1.000	0.696	1.000	1.000	0.666	1.000	1.000	0.634	1.000	1.000	0.604	1.000	1.000	0.590	1.000
	3 clusters	1.000	0.687	1.000	1.000	0.656	1.000	1.000	0.627	1.000	1.000	0.599	1.000	1.000	0.587	1.000
	5 clusters	0.997	0.633	0.996	0.999	0.598	1.000	0.999	0.570	1.000	1.000	0.547	1.000	1.000	0.535	1.000

Table 3: The simulation results of KS-CCDs on a set of synthetic datasets consisting of uniform clusters. While KS-CCDs generally provide superior clustering performance, their effectiveness drops significantly when identifying a high number of clusters in a small dataset due to low cluster intensity.

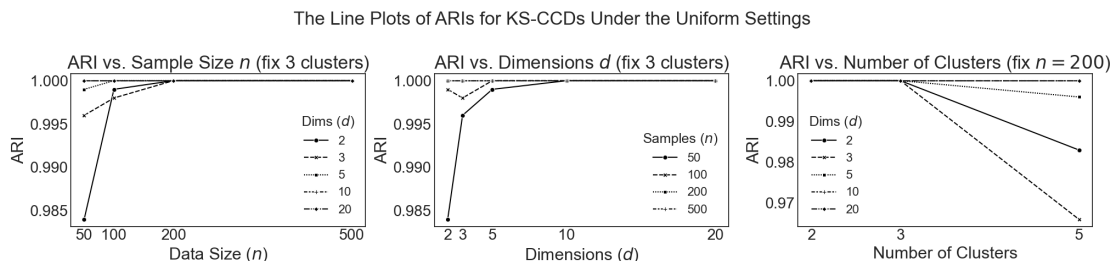


Figure 3: The line plots of the ARIs of KS-CCDs, under the uniform cluster settings.

RK-CCDs		d = 2			d = 3			d = 5			d = 10			d = 20		
		ARI	Sil	SR	ARI	Sil	SR	ARI	Sil	SR	ARI	Sil	SR	ARI	Sil	SR
$n = 50$	2 clusters	0.982	0.692	0.998	0.999	0.665	1.000	0.997	0.630	0.992	0.988	0.596	0.960	0.833	0.444	0.474
	3 clusters	0.906	0.655	0.844	0.990	0.651	0.988	0.998	0.625	0.994	0.972	0.589	0.920	0.681	0.424	0.382
	5 clusters	0.517	0.484	0.082	0.810	0.556	0.424	0.967	0.563	0.908	0.994	0.544	0.968	0.801	0.473	0.410
$n = 100$	2 clusters	0.999	0.697	1.000	0.999	0.665	1.000	0.999	0.633	0.998	0.979	0.584	0.922	0.834	0.437	0.454
	3 clusters	0.992	0.684	0.988	0.999	0.654	0.998	0.996	0.624	0.990	0.951	0.576	0.852	0.684	0.433	0.302
	5 clusters	0.768	0.567	0.302	0.938	0.585	0.792	0.982	0.564	0.958	0.956	0.531	0.796	0.511	0.373	0.080
$n = 200$	2 clusters	0.999	0.698	1.000	1.000	0.666	1.000	1.000	0.631	1.000	0.972	0.576	0.892	0.758	0.384	0.288
	3 clusters	1.000	0.688	1.000	0.999	0.655	1.000	1.000	0.626	1.000	0.912	0.560	0.740	0.597	0.376	0.312
	5 clusters	0.926	0.610	0.748	0.988	0.595	0.968	0.993	0.568	0.976	0.917	0.513	0.626	0.595	0.391	0.130
$n = 500$	2 clusters	1.000	0.696	1.000	1.000	0.669	1.000	1.000	0.634	1.000	0.976	0.579	0.910	0.787	0.419	0.428
	3 clusters	0.999	0.686	1.000	1.000	0.654	1.000	1.000	0.627	1.000	0.929	0.571	0.806	0.592	0.394	0.208
	5 clusters	0.997	0.632	1.000	0.999	0.600	1.000	0.999	0.570	1.000	0.865	0.498	0.494	0.439	0.344	0.082

Table 4: The simulation results of RK-CCDs on a set of synthetic datasets consisting of uniform clusters. The performance of RK-CCDs declines sharply in high-dimensional spaces due to the limitation of the Ripley’s K function.

The Line Plots of ARIs for RK-CCDs Under the Uniform Settings

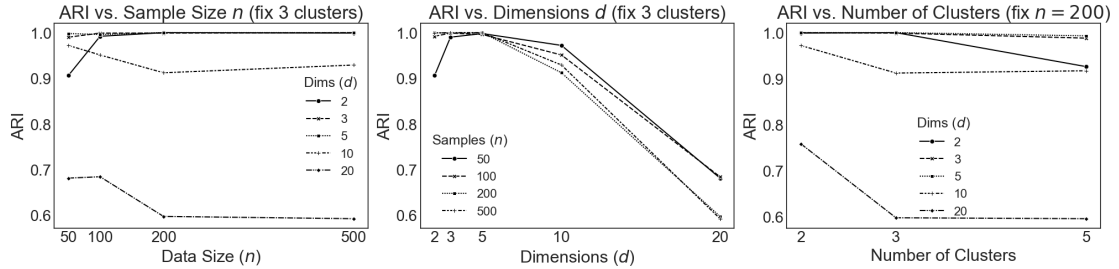


Figure 4: The line plots of the ARIs of RK-CCDs, under the uniform cluster settings.

According to the simulation result, KS-CCDs consistently deliver superior performance when the optimal δ is selected, yielding *ARI* values and success rates (*SR*) close to 1 across most simulation settings, resulting in high average *Sil* values (consistently above 0.55). However, in certain cases when $n = 50$, KS-CCDs exhibit reduced efficiency when dealing with 5 clusters. For example, when $d = 2$ and $n = 50$, the success rate (*SR*) declines from 0.998 to 0.622 as the number of clusters increases from 2 to 5. As shown in the Figure 3, the ARI value also decreases when the number of cluster increase. The degradation in performance can be attributed to a drop in the intensities of individual clusters. Furthermore, the small proximity of the 4th and 5th clusters to the

The Line Plots of ARIs for UN-CCDs Under the Uniform Settings

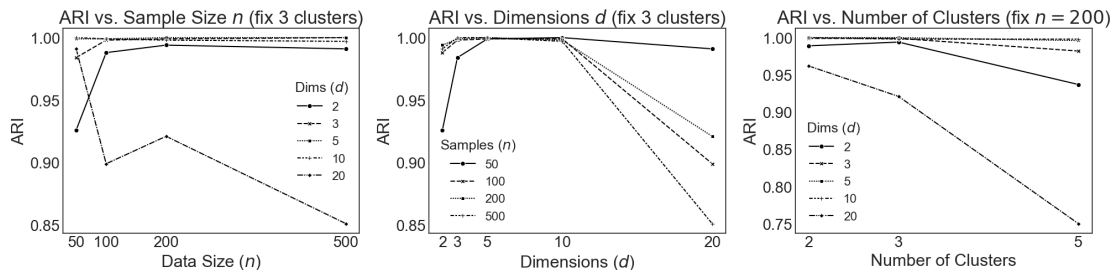


Figure 5: The line plots of the ARIs of UN-CCDs, under the uniform cluster settings.

UN-CCDs			d = 2			d = 3			d = 5			d = 10			d = 20		
			ARI	Sil	SR	ARI	Sil	SR	ARI	Sil	SR	ARI	Sil	SR	ARI	Sil	SR
$n = 50$	2 clusters	0.980	0.691	0.996	0.996	0.664	1.000	0.999	0.632	1.000	1.000	0.608	1.000	0.992	0.585	0.968	
	3 clusters	0.926	0.658	0.902	0.981	0.649	0.972	0.999	0.626	1.000	1.000	0.600	1.000	0.991	0.580	0.972	
	5 clusters	0.610	0.511	0.214	0.795	0.549	0.480	0.951	0.560	0.872	0.996	0.546	0.992	0.991	0.531	0.944	
$n = 100$	2 clusters	0.992	0.695	0.998	0.999	0.665	1.000	1.000	0.634	1.000	1.000	0.606	1.000	0.957	0.545	0.840	
	3 clusters	0.988	0.682	0.988	0.998	0.654	1.000	0.999	0.625	0.998	0.999	0.598	0.998	0.899	0.540	0.726	
	5 clusters	0.847	0.583	0.604	0.935	0.582	0.836	0.986	0.565	0.976	0.998	0.546	0.992	0.957	0.521	0.802	
$n = 200$	2 clusters	0.989	0.694	0.996	0.999	0.665	1.000	1.000	0.631	1.000	1.000	0.606	1.000	0.962	0.547	0.848	
	3 clusters	0.994	0.685	0.998	0.999	0.655	1.000	1.000	0.626	1.000	0.998	0.600	0.996	0.921	0.558	0.802	
	5 clusters	0.937	0.608	0.858	0.982	0.592	0.968	0.996	0.560	0.996	0.998	0.547	0.990	0.750	0.460	0.284	
$n = 500$	2 clusters	0.992	0.693	0.998	1.000	0.666	1.000	1.000	0.634	1.000	1.000	0.604	1.000	0.962	0.548	0.850	
	3 clusters	0.991	0.682	1.000	1.000	0.655	1.000	1.000	0.627	1.000	0.997	0.597	0.990	0.851	0.525	0.610	
	5 clusters	0.978	0.624	0.974	0.996	0.597	0.998	0.999	0.570	1.000	0.997	0.545	0.982	0.844	0.477	0.438	

Table 5: The simulation results of UN-CCDs on a set of synthetic datasets consisting of uniform clusters. UN-CCDs perform comparably to RK-CCDs in low dimensions but are substantially superior in high dimensions.

existing clusters increases the likelihood of these clusters being erroneously confused as one. Fortunately, when $n \geq 100$, KS-CCDs exhibit substantial improvement in handling 5-cluster datasets.

Although RK-CCDs are not as effective as KS-CCDs across lower-dimensional settings ($d \leq 5$), they still maintain *ARI* values and success rates (*SR*) above 0.9 in most scenarios, indicating solid performance in low-dimensional space. However, similar to the behavior of KS-CCDs, RK-CCDs also suffer performance degradation in certain cases when there are 5 clusters. For instance, when $d = 2$ and $n = 50$, the success rate (*SR*) drops drastically from 0.998 to 0.082 as the number of clusters increases from 2 to 5, attributable to the low intensities of individual clusters. Additionally, RK-CCDs perform worse in high-dimensional space, due to the limitations of the Ripley’s K function when d is large. for example, when $d = 10$, the success rates (*SR*) decrease substantially, reaching a minimum of 0.494 for 5-cluster datasets when $n = 500$. This deterioration is further exacerbated when $d = 20$, with *ARI* values falling below 0.8 and success rates (*SR*) smaller than 0.4 in most settings.

Under low-dimensional space ($d \leq 5$), UN-CCDs demonstrate comparable performance to RK-CCDs, achieving *ARI* values and success rates (*SR*) exceeding 0.95 in most settings. Furthermore, UN-CCDs exhibit substantial improvement over RK-CCDs in high-dimensional space. When $d = 10$, both *ARI* and success rate approach 1, much higher than those achieved by RK-CCDs. The performance gap between RK-CCDs and UN-CCDs becomes even more pronounced when $d = 20$. For example, with 3-cluster datasets where $n = 200$, UN-CCDs yield performance metrics of 0.921 (*ARI*), 0.558 (*Sil*), and 0.802 (success rate), respectively. These values are substantially higher than the corresponding 0.597, 0.376, and 0.312 obtained by RK-CCDs. As we talked previously in Section 3.2, this improvement is attributed to the newly developed MC-SRT,

which employed NND instead of the Ripley's K function with several additional key enhancements.

4.2 Experiment with Gaussian Settings

Assuming CSR, UN-CCDs and RK-CCDs perform well with uniform clusters. To evaluate the performance of CCD-based clustering methods on non-uniform data, we conduct simulations with Gaussian clusters. Each Gaussian cluster has a covariance matrix $\Delta * I_d$, where Δ is a random uniform variable between 0.8 and 1.2 (for random scaling), and I_d represents a $d \times d$ identity matrix. All other settings, including dimensionality, data size, cluster centers, and the number of clusters, remain the same as in the uniform settings. Three realizations with different number of Gaussian clusters ($d = 2$) are presented in Figure 6. The simulation results are summarized in Table 7, 8, and 9. Similarly, we present the performance trend (ARIs) of the CCD-based methods from Figures 7 to 9.

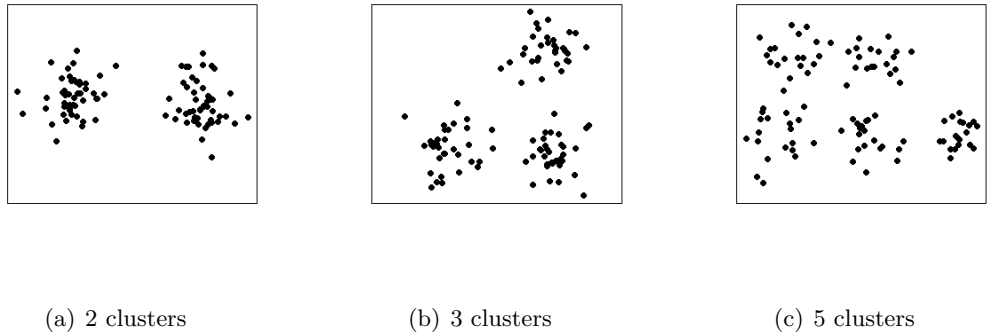


Figure 6: Realizations of the simulation settings with 2, 3, and 5 Gaussian clusters in \mathbb{R}^2 .

Density Parameter: $\sqrt[d]{\delta}$		$d = 2$	$d = 3$	$d = 5$	$d = 10$	$d = 20$
$n = 50$	2 clusters	1.90	1.10	0.60	0.32	0.20
	3 clusters	1.60	0.93	0.52	0.30	0.19
	5 clusters	1.30	0.79	0.46	0.28	0.18
$n = 100$	2 clusters	3.00	1.40	0.71	0.35	0.21
	3 clusters	2.30	1.20	0.65	0.32	0.20
	5 clusters	1.90	0.99	0.58	0.32	0.17
$n = 200$	2 clusters	4.20	1.70	0.76	0.39	0.23
	3 clusters	3.50	1.50	0.71	0.37	0.21
	5 clusters	2.70	1.30	0.66	0.35	0.17
$n = 500$	2 clusters	7.1	2.5	0.95	0.43	0.24
	3 clusters	5.6	2.1	0.90	0.41	0.24
	5 clusters	4.3	1.8	0.82	0.41	0.19

Table 6: The optimal scaled densities ($\sqrt[d]{\delta}$) of KS-CCDs on synthetic datasets consisting of Gaussian clusters.

KS-CCDs		d = 2			d = 3			d = 5			d = 10			d = 20		
		ARI	Sil	SR	ARI	Sil	SR	ARI	Sil	SR	ARI	Sil	SR	ARI	Sil	SR
$n = 50$	2 clusters	0.983	0.704	1.000	0.980	0.633	1.000	0.974	0.537	1.000	0.947	0.399	1.000	0.798	0.247	0.960
	3 clusters	0.973	0.688	0.984	0.970	0.619	0.986	0.960	0.524	0.970	0.880	0.381	0.832	0.685	0.251	0.470
	5 clusters	0.936	0.644	0.890	0.921	0.569	0.872	0.865	0.470	0.718	0.651	0.338	0.376	0.380	0.244	0.050
$n = 100$	2 clusters	0.980	0.704	1.000	0.987	0.635	1.000	0.982	0.540	1.000	0.960	0.399	0.998	0.846	0.256	0.980
	3 clusters	0.985	0.693	1.000	0.981	0.621	0.996	0.978	0.527	0.996	0.926	0.383	0.920	0.713	0.254	0.508
	5 clusters	0.963	0.652	0.986	0.962	0.582	0.982	0.939	0.475	0.936	0.717	0.341	0.556	0.303	0.249	0.000
$n = 200$	2 clusters	0.988	0.703	1.000	0.988	0.634	1.000	0.987	0.539	1.000	0.970	0.402	1.000	0.878	0.261	0.982
	3 clusters	0.988	0.694	1.000	0.988	0.623	1.000	0.984	0.527	1.000	0.963	0.389	0.988	0.736	0.257	0.550
	5 clusters	0.977	0.657	0.998	0.973	0.581	0.998	0.965	0.481	0.988	0.778	0.342	0.704	0.263	0.254	0.000
$n = 500$	2 clusters	0.990	0.703	1.000	0.991	0.637	1.000	0.989	0.541	1.000	0.978	0.404	1.000	0.905	0.266	0.998
	3 clusters	0.989	0.691	1.000	0.990	0.625	1.000	0.988	0.528	1.000	0.976	0.391	0.996	0.793	0.258	0.652
	5 clusters	0.981	0.658	1.000	0.980	0.586	1.000	0.974	0.483	1.000	0.824	0.347	0.776	0.297	0.255	0.000

Table 7: The simulation results of KS-CCDs on a set of synthetic datasets consisting of Gaussian clusters. While highly efficient with Gaussian clusters in low dimensions, KS-CCDs’ performance degrades substantially in high-dimensional spaces due to the decreased intensity and unbounded nature of Gaussian distributions.

The Line Plots of ARIs for KS-CCDs Under the Gaussian Settings

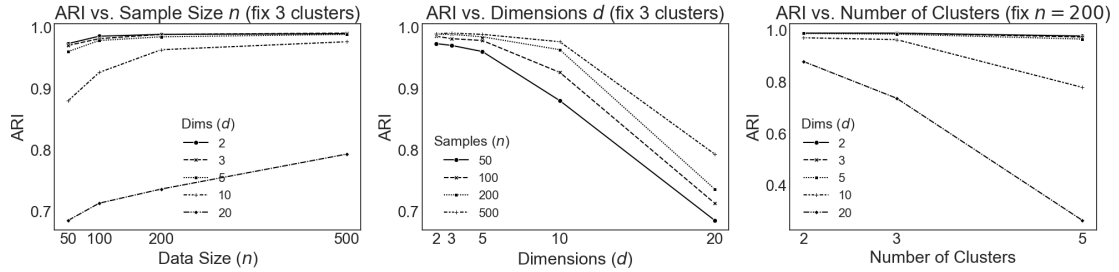


Figure 7: The line plots of the ARIs of KS-CCDs, under the Gaussian cluster settings.

While the optimal density parameter δ is selected for each simulation setting, KS-CCDs demonstrate reduced effectiveness with Gaussian clusters. In low-dimensional settings ($d \leq 5$), KS-CCDs deliver slightly lower performance in the comparable scenarios with uniform clusters. Notably, *ARI* values and success rates (*SR*) remain high (> 0.95), indicating high efficiency even with Gaussian clusters. However, as shown in the second line plot of Figure 7, KS-CCDs degrade substantially in high-dimensional settings ($d \geq 10$), particularly with three or more clusters. For example, when $d = 20$ and $n = 200$, KS-CCDs deliver average performance metrics of 0.736 (*ARI*), 0.257 (*Sil*),

The Line Plots of ARIs for RK-CCDs Under the Gaussian Settings

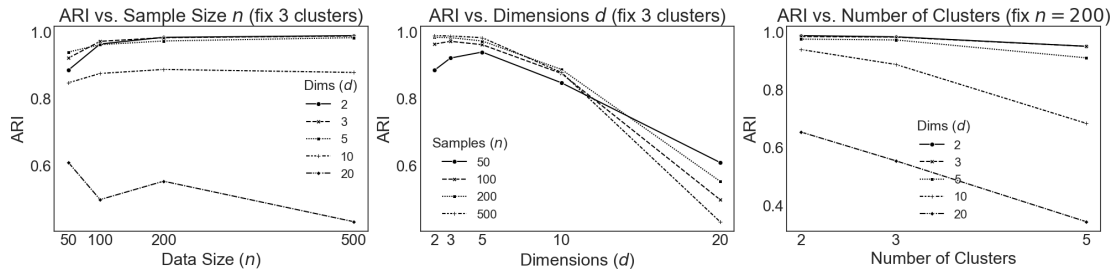


Figure 8: The line plots of the ARIs of RK-CCDs, under the Gaussian cluster settings.

KS-CCDs		d = 2			d = 3			d = 5			d = 10			d = 20		
		ARI	Sil	SR	ARI	Sil	SR	ARI	Sil	SR	ARI	Sil	SR	ARI	Sil	SR
$n = 50$	2 clusters	0.950	0.691	1.000	0.964	0.627	1.000	0.949	0.528	0.994	0.908	0.384	0.978	0.660	0.181	0.628
	3 clusters	0.885	0.659	0.812	0.921	0.607	0.882	0.939	0.517	0.944	0.847	0.372	0.784	0.609	0.212	0.304
	5 clusters	0.627	0.535	0.232	0.760	0.521	0.448	0.812	0.453	0.646	0.654	0.328	0.452	0.396	0.222	0.078
$n = 100$	2 clusters	0.982	0.702	1.000	0.980	0.632	1.000	0.972	0.536	0.998	0.917	0.381	0.958	0.664	0.181	0.630
	3 clusters	0.963	0.685	0.962	0.971	0.617	0.984	0.961	0.521	0.978	0.875	0.370	0.814	0.498	0.186	0.218
	5 clusters	0.830	0.600	0.594	0.906	0.561	0.798	0.874	0.459	0.802	0.664	0.327	0.462	0.348	0.199	0.046
$n = 200$	2 clusters	0.987	0.702	1.000	0.984	0.633	1.000	0.975	0.535	1.000	0.939	0.387	0.954	0.653	0.170	0.548
	3 clusters	0.983	0.692	0.998	0.982	0.621	0.998	0.972	0.522	0.988	0.887	0.375	0.826	0.553	0.188	0.272
	5 clusters	0.950	0.646	0.934	0.950	0.572	0.932	0.910	0.467	0.870	0.683	0.328	0.500	0.342	0.201	0.048
$n = 500$	2 clusters	0.989	0.702	1.000	0.990	0.633	1.000	0.984	0.540	1.000	0.939	0.383	0.912	0.578	0.152	0.500
	3 clusters	0.988	0.690	1.000	0.987	0.624	1.000	0.982	0.525	0.996	0.878	0.370	0.780	0.432	0.165	0.174
	5 clusters	0.977	0.655	0.994	0.976	0.581	1.000	0.951	0.475	0.960	0.668	0.328	0.454	0.335	0.184	0.066

Table 8: The simulation results of RK-CCDs on a set of synthetic datasets consisting of Gaussian clusters. Similar to Uniform settings, the performance of RK-CCDs deteriorates significantly in high-dimensional space due to the limitations of the Ripley’s K function.

UN-CCDs		d = 2			d = 3			d = 5			d = 10			d = 20		
		ARI	Sil	SR	ARI	Sil	SR	ARI	Sil	SR	ARI	Sil	SR	ARI	Sil	SR
$n = 50$	2 clusters	0.930	0.683	0.988	0.958	0.625	1.000	0.953	0.530	0.998	0.943	0.395	1.000	0.850	0.249	0.988
	3 clusters	0.868	0.649	0.854	0.910	0.600	0.912	0.939	0.517	0.944	0.864	0.374	0.820	0.740	0.248	0.574
	5 clusters	0.644	0.524	0.346	0.740	0.515	0.470	0.774	0.446	0.578	0.600	0.330	0.320	0.444	0.232	0.136
$n = 100$	2 clusters	0.960	0.695	0.994	0.971	0.630	0.998	0.974	0.537	1.000	0.951	0.394	1.000	0.859	0.248	0.962
	3 clusters	0.941	0.676	0.958	0.959	0.612	0.978	0.963	0.522	0.984	0.917	0.379	0.904	0.765	0.247	0.618
	5 clusters	0.828	0.593	0.670	0.888	0.555	0.816	0.875	0.462	0.810	0.713	0.336	0.554	0.438	0.232	0.128
$n = 200$	2 clusters	0.967	0.696	1.000	0.977	0.631	1.000	0.979	0.537	1.000	0.963	0.399	1.000	0.875	0.254	0.978
	3 clusters	0.967	0.685	0.996	0.972	0.618	0.996	0.978	0.524	1.000	0.955	0.386	0.972	0.758	0.250	0.586
	5 clusters	0.913	0.628	0.902	0.942	0.569	0.950	0.939	0.473	0.952	0.750	0.337	0.648	0.439	0.235	0.134
$n = 500$	2 clusters	0.971	0.697	1.000	0.982	0.635	1.000	0.983	0.540	1.000	0.973	0.402	1.000	0.885	0.253	0.946
	3 clusters	0.968	0.683	0.996	0.981	0.621	1.000	0.981	0.525	1.000	0.965	0.387	0.988	0.799	0.249	0.662
	5 clusters	0.950	0.643	0.984	0.963	0.578	0.994	0.963	0.477	0.998	0.808	0.342	0.760	0.450	0.232	0.140

Table 9: The simulation results of UN-CCDs on a set of synthetic datasets consisting of Gaussian clusters. The UN-CCD method demonstrate substantial advantage over KS-CCDs and RK-CCDs in high-dimensional space.

and 0.550 (success rate) for 3-cluster datasets, drastically lower than the corresponding 1, 0.587, and 1 obtained with uniform clusters. This performance decline can be explained by the decreased intensities of Gaussian clusters in high-dimensional space, an effect amplified with a larger number of clusters (e.g., 5 clusters), suggested by the third line plot of Figure 7. Moreover, the support of Gaussian clusters is unbounded, further contributes to the performance degradation.

Similar to the simulations with uniform clusters, RK-CCDs generally perform well

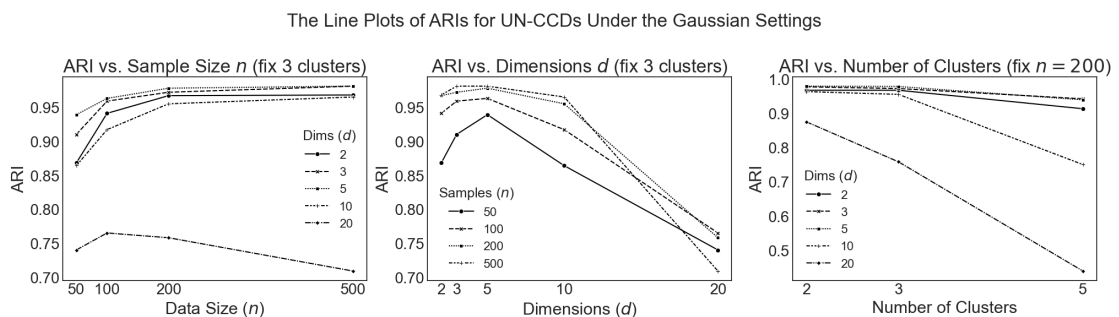


Figure 9: The line plots of the ARIs of UN-CCDs, under the Gaussian cluster settings.

in low-dimensional space, with ARI values and success rates (SR) exceeding 0.9 except certain cases with 5 clusters, where the proximities between clusters and the intensities of individual clusters are small. For instance, with $d = 2$, $n = 50$, and 5 clusters, the performance metrics of RK-CCDs are 0.627 (ARI), 0.535 (Sil), and 0.234 (success rate), respectively. RK-CCDs demonstrate similar behavior in high-dimensional space ($d \geq 10$) as in the uniform settings. Their performance is slightly worse than KS-CCDs when $d = 10$, and deteriorate further when $d = 20$, increasing the data size does not help. For example, when $d = 20$ and $n = 500$, the ARI and success rate are 0.297 and 0, respectively, due to the limitations of the MC-SRT based on the Ripley's K function.

Similar to the previous analysis, UN-CCDs perform similarly to RK-CCDs and KS-CCDs in low-dimensional space ($d \leq 5$), Both ARI values and success rates exceed 0.9 in most scenarios, with a few exceptions observed when dealing with 5 clusters. These results are slightly lower than those obtained with uniform clusters. However, UN-CCDs yield superior overall performance in high-dimensional space ($d \geq 10$). When $d = 10$, UN-CCDs deliver comparable performance to KS-CCDs, outperforming RK-CCDs, as evidenced by higher ARI values and success rates. To illustrate, with $n = 200$, $d = 10$, and 3 clusters, the ARI values for KS-CCDs, RK-CCDs, and UN-CCDs are 0.963, 0.877, and 0.955, respectively. Furthermore, UN-CCDs exhibit a substantial advantage over the other two CCDs when $d = 20$. For example, with $n = 200$, $d = 20$, and 5 clusters, the ARI values for KS-CCDs, RK-CCDs, and UN-CCDs are 0.263, 0.342, and 0.439, respectively.

To summarize, KS-CCDs demonstrate the best overall performance with uniform clusters when the optimal density parameter δ is selected, achieving ARI values and success rates close to 1 in most scenarios, invariant to the dimensionality d . UN-CCDs exhibit slightly lower performance compared to KS-CCDs, and show a substantial advantage over RK-CCDs when $d \geq 10$. All three CCDs perform slightly worse with Gaussian clusters in low-dimensional space ($d \leq 5$), further deteriorate when $d \geq 10$, where UN-CCDs outperform both RK-CCDs and KS-CCDs. The performance of all three CCDs declines with 5 clusters, particularly when the data size n is small. This is attributed to the low intensities of individual clusters and the small proximities between clusters.

4.3 Experiment on Datasets with Noise

In this section, we conduct additional simulation experiments to evaluate whether the UN-CCD method is robust to noise. The general simulation setup is similar to the experiments with Gaussian settings, where each Gaussian cluster has a random scaling covariance matrix $\Delta * I_d$. To simplify the study, we set the number of clusters to 3, and the data size to 200 plus the number of noise points. Noise refers to the points that are randomly distributed within the scope of the entire dataset. we simulate datasets with varying noise level (3%, 5%, 10%, 20%) to assess the performance trend of UN-CCD methods. Additionally, we consider both 3-dimensional and 10-dimensional datasets to study the impact of noise level with different dimensions. Specific details are outlined below. Some realizations of datasets with Gaussian clusters in 2-dimensional space (although the simulation experiments are conducted on 3 and 10-dimensional space) are presented in Figure 10 (for illustration purposes). Similar to the previous simulation study, Each simulation setting is repeated 1000 times to ensure accurate results. The simulation results are summarized in Table 10, similar to the previous simulations, we record the average *ARI*, *Sil*, and *SR* under each setting.

- i. The dimensionality (d) of the simulated datasets: 3, 10;
- ii. The noise levels (l): 3%, 5%, 10%, 20%
- iii. The size of datasets (n): $200 \times (1 + l)$;
- iv. The size of each cluster is equal;
- v. The number of clusters: 3;
- vi. The centers of Gaussian clusters: $\mu_1 = (\underbrace{3, \dots, 3}_d)$, $\mu_2 = (9, \underbrace{3, \dots, 3}_{d-1})$, and $\mu_3 = (3, \underbrace{9, 3, \dots, 3}_{d-2})$.
- vii. The covariance matrix of each Gaussian cluster: $\Delta * I_d$, where $\Delta \sim U[0.8, 1.2]$ and I_d is a d -dimensional identity matrix.

The UN-CCD method is highly robust to noise, maintaining consistent performance across various noise levels. Specifically, when $d = 3$, increasing the noise level (l) from 3% to 20% has a negligible effect. For example, the *ARI* values are 0.977, 0.977, 0.975, and 0.971 when l increases from 3% to 20%; meanwhile, the Success Rate (*SR*) only slightly decreases from 1.000 to 0.982. While the effect of noise is greater when $d = 10$,

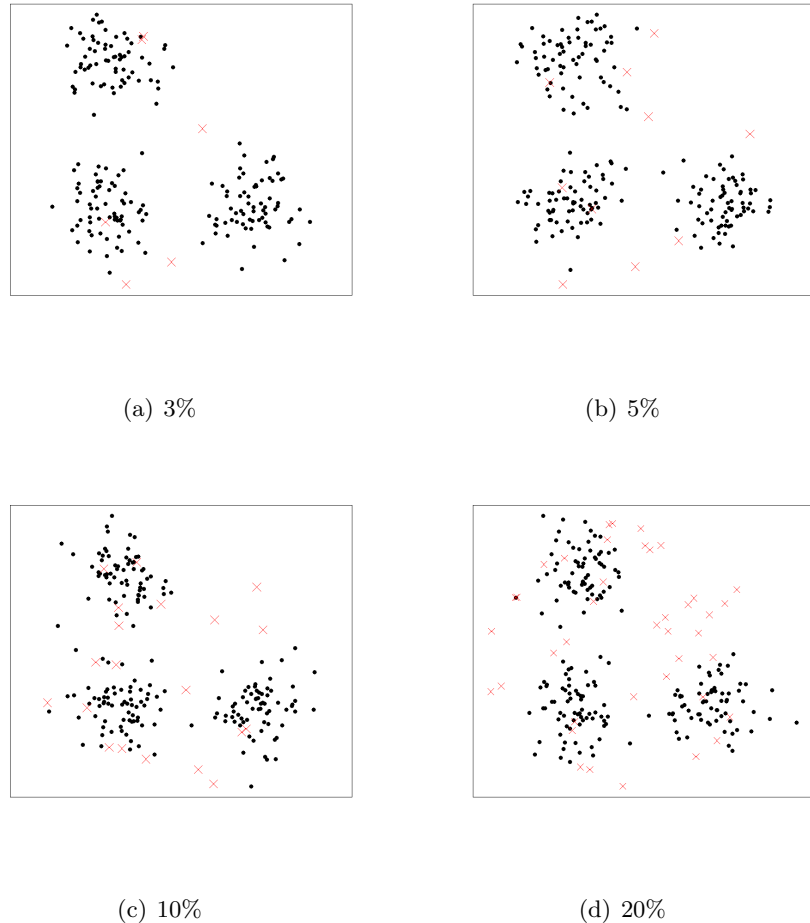


Figure 10: Some realizations of the simulation studying the impact of different noise levels, the noise level varies from 3% to 20%. Red crosses are noise, black points are regular observations. The noise levels are indicated below each sub-figure.

the method remains effective, with the SR decreasing from 0.973 to 0.942. Overall, these results demonstrate the UN-CCD's reliable performance in the presence of noise across various dimensions.

5 Real Data Examples

We assess the performance of three CCD-based clustering methods using some benchmark real and synthetic datasets in this section, and compare them with some well-known, established clustering methods. Moreover, we want to explore if UN-CCDs outperform RK-CCDs after multiple enhancements. The datasets, obtained from **UCI Machine Learning Repository** and **Clustering basic benchmark** [17, 23], are generally more complex in the data structure, thus more challenging for clustering than the datasets used in Section 4. To prevent features with larger scales from dominating, we

UN-CCDs	$l = 3\%$			$l = 5\%$			$l = 10\%$			$l = 20\%$		
	<i>ARI</i>	<i>Sil</i>	<i>SR</i>									
$d = 3$	0.977	0.619	1.000	0.977	0.619	1.000	0.975	0.618	0.998	0.971	0.617	0.982
$d = 10$	0.959	0.386	0.973	0.961	0.384	0.977	0.954	0.384	0.960	0.947	0.385	0.942

Table 10: The simulation results of UN-CCDs on a set of synthetic datasets with varying noise level and 3 Gaussian clusters, demonstrating that the UN-CCD method is invariant to varying noise levels.

preprocess the datasets by normalizing them (except the synthetic datasets, including “asymmetric”, “R15”, and “D31” datasets).

The details and background of each dataset are summarized below. Moreover, we present the “asymmetric”, “R15”, and “D31” datasets in Figure 11. We are treating all datasets unlabeled, and compare the obtained clusters with the classes already available in the datasets.

Brief descriptions of each dataset.

- **iris:** A dataset of iris plant, containing 3 types of 50 instances for each.
- **seeds:** The measurements of geometrical properties of kernels belonging to 3 different wheat varieties.
- **knowledge:** Measures the students’ knowledge of Electrical DC Machines, categorized into 4 levels.
- **wholesale:** This dataset refers to clients of a wholesale distributor, it includes the clients’ annual spending on diverse product categories, and are grouped to 3 regions.
- **asymmetric:** A synthetic 2-dimensional datasets with 5 elliptical Gaussian clusters of unbalanced cluster size and intensities, and the inter-cluster distances varies [49].
- **R15 and D31:** Synthetic datasets consist of 15 or 31 similar Gaussian clusters [61]

We compare the performance of CCDs with established clustering algorithms, **Density Based Spatial Clustering of Applications with Noise** (DBSCAN) [20], the **Minimal Spanning Tree** (MST) Method [70], **Spectral Clustering** (Spectral) [42], **K-means++** [3], and **Louvain Clustering Method** (Louvain) [8].

DBSCAN is a density-based clustering method proposed by Ester *et al.* [20], often used to handle datasets with noise or outliers. It identifies clusters by finding “seeds”,

	n	d	# of clusters
iris	150	4	3
seeds	210	7	3
knowledge	258	6	4
wholesale	440	8	3
R15	600	2	15
asymmetric	1000	2	5
D31	3100	2	31

Table 11: The size (n), dimensionality (d), and contamination level of each real-life dataset.

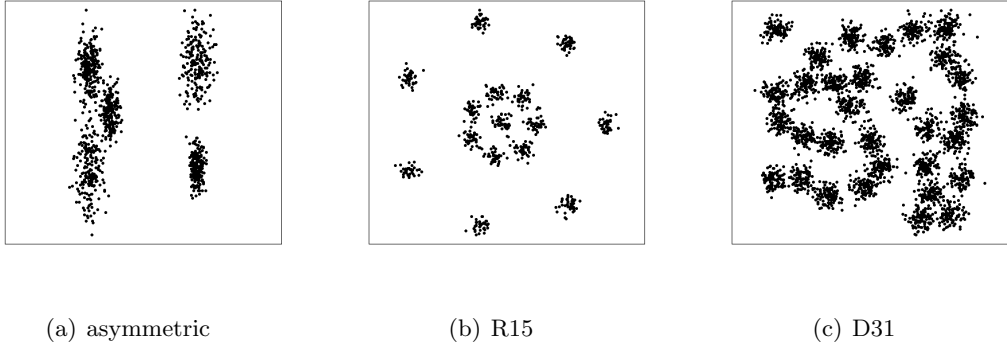


Figure 11: The figures of asymmetric, R15, and D31 datasets

which are the points deep inside clusters that have a minimum number (denoted as **MinPts**) of neighbors within a given radius (denoted as **Eps**). After that, it constructs clusters by finding all the points that are **density-reachable** from seeds. Finally, the points not connected to any seeds are labeled as noise or outliers. **MinPts** and **Eps** are the two input parameters, we follow a heuristic offered by Ester *et al.*, which sets **MinPts** to 4, and find the value at the first “elbow” of the sorted 4-dist (the distance of a point to its 4th nearest neighbor) plot, setting it to **Eps** [20].

The MST clustering method employs a graph-based approach [70]. This method involves constructing a graph by connecting all data points with the minimum sum of edge weights, typically represented by the distance between two points. Subsequently, edges with significantly larger weights than their adjacent edges’ average weight are identified as “inconsistent” and removed. This removal effectively breaks the MST into subtrees, each representing a distinct cluster. After the trial-and-error process, We set the threshold value for “inconsistent” edges to 2, which delivers the best overall performance compared to other thresholds.

Spectral clustering starts by constructing a similarity matrix of the given dataset [42]. Then, it derives the Laplacian matrix from the similarity matrix, and the eigenvalues of the Laplacian matrix provide a low-dimensional embedding of the original data. Finally,

it applies a traditional method for clustering. In our experiment, we chose Gaussian similarity function to define the similarity and K -means for clustering, with the number of clusters k as the input parameter.

K -means++ enhances the classic K -means clustering method [3]. A key weakness of K -means is the sensitivity to the initially chosen cluster centroids. K -means++ addresses this limitation by selecting initial centroids that are far apart, leading to better and more stable clustering results and faster convergence. Similar to spectral clustering, we conduct K -means++ on each dataset with the true number of clusters as an input.

Louvain clustering method is a greedy algorithm finding communities in large networks by maximizing the “modularity”, which measures the quality of a partition[8]. The algorithm first optimizes modularity by iteratively moving individual nodes between communities, then aggregates these communities into new nodes and repeats the process until no further improvement is possible. In this experiment, we first employ the standardized Gaussian kernel to construct a network for the given dataset, and then apply the Louvain clustering method with the default resolution parameter to find the communities (i.e., 1).

Consider the CCD-based methods, α is set to 1% for all the dataset for simplicity. For KS-CCDs, we choose the $\sqrt[d]{\delta}$ value that maximizes the average silhouette index in each dataset.

We choose the Adjust Rand Index and Silhouette Index as external and internal validation measures. Furthermore, we record the number of clusters detected by each method. The performance of all methods is summarized in Table 12.

	iris ($k=3$)			seeds ($k=3$)			knowledge ($k=3$)			wholesale ($k=3$)			asymmetric ($k=5$)			R15 ($k = 15$)			D31 ($k = 31$)		
	<i>ARI</i>	<i>Sil</i>	k	<i>ARI</i>	<i>Sil</i>	k	<i>ARI</i>	<i>Sil</i>	k	<i>ARI</i>	<i>Sil</i>	k	<i>ARI</i>	<i>Sil</i>	k	<i>ARI</i>	<i>Sil</i>	k	<i>ARI</i>	<i>Sil</i>	k
KS-CCDs	0.561	0.578	2	0.497	0.468	2	0.005	0.254	2	-0.013	0.765	2	0.691	0.643	4	0.989	0.753	15	0.948	0.574	31
RK-CCDs	0.557	0.393	3	0.500	0.164	3	0.052	0.119	2	-0.002	0.344	2	0.730	0.605	4	0.993	0.753	15	0.814	0.495	30
UN-CCDs	0.599	0.445	3	0.509	0.467	2	0.091	0.158	2	0.002	0.113	3	0.736	0.606	4	0.975	0.742	15	0.799	0.474	31
DBSCAN	0.544	0.517	2	0.003	0.121	1	0.005	0.198	1	0.006	0.569	1	0.467	0.548	3	0.936	0.702	15	0.350	0.343	15
MST	0.530	-0.145	6	0.000	-0.364	4	0.003	-0.089	3	0.004	-0.491	13	0.785	-0.160	12	0.536	-0.071	65	0.511	-0.199	276
K-mean++	0.590	0.459	3*	0.773	0.404	3*	0.202	0.169	4*	-0.007	0.446	3*	0.882	0.645	5*	0.894	0.678	15*	0.912	0.547	31*
Spectral	0.555	0.475	3*	0.679	0.349	3*	0.189	0.120	4*	-0.012	0.446	3*	0.975	0.623	5*	0.899	0.611	15*	0.778	0.332	31*
Louvain	0.630	0.436	3	0.722	0.394	3	0.149	0.155	5	-0.004	0.243	6	0.805	0.479	8	0.604	0.644	10	0.371	0.446	9

Table 12: The performance of selected clustering algorithms on real and complex datasets. *ARI*: Adjust Rand Index; *Sil*: Silhouette Index; k : number of clusters (k is the input parameter for K-mean++ and spectral clustering); \hat{k} : estimated number of clusters.

“iris” datasets: Except MST, all the methods obtain comparable *ARIs* on the “iris” dataset. Precisely, Louvain and UN-CCDs attain the highest *ARIs* of 0.630 and 0.599, respectively. KS-CCDs and DBSCAN produce the best *Sil* values. RK-CCDs, UN-

CCDs, and Louvain clustering method correctly identify the true number of clusters. MST’s underperformance is due to its sensitivity to the varying intensities of the iris clusters.

“seeds” datasets: In the “seeds” dataset, K -means++, spectral clustering, and Louvain clustering method perform better than other methods when considering ARI . On the other hand, UN-CCDs and KS-CCDs achieve the highest Sil values of 0.468 and 0.467, respectively, indicating better-defined cluster structures. Both RK-CCDs and Louvain clustering method successfully identify the correct number of clusters. DBSCAN underperforms due to the difficulty to find a single **Eps** value that works globally.

“knowledge” dataset: In the “knowledge” dataset, The performance of all the methods is generally mediocre. K -mean++ and spectral clustering get the highest ARI values, 0.202 and 0.189, respectively. KS-CCDs and DBSCAN produce the best Sil values. MST is the only method that identified 3 clusters.

“wholesale” dataset: All the methods perform poorly on the “wholesale” dataset, Suggested by the $ARIs$, which are around 0, indicating the clustering results akin to random assignment. Therefore, we consider Sil for evaluation, KS-CCDs and DBSCAN outperform other methods, achieving Sil values of 0.765 and 0.569, respectively. Despite having the second-lowest Sil value (0.113), UN-CCDs is the only method that correctly identifies the number of clusters.

“asymmetric” dataset: When the number of clusters is known, K -means++ and spectral clustering exhibit the best performance on the “asymmetric” dataset. These methods achieve ARI values of 0.882 and 0.975, respectively, and Sil values of 0.645 and 0.623, respectively. The CCD-based methods show slightly lower performance, with ARI and Sil values around 0.7 and 0.6, respectively. However, these methods identify 4 clusters, the closest to the actual number.

“R15” dataset: The three CCD-based methods perform better than the other methods on the “R15” dataset, they successfully capture 15 Gaussian clusters, achieving ARI values close to 1 and Sil values around 0.75. DBSCAN, K -means++, and spectral clustering deliver slightly inferior performance, with ARI values around 0.9 and Sil values around 0.65.

“D31” dataset: Consider the “D31” dataset, KS-CCDs and K -means++ detect all 31 clusters, deliver the highest ARI values of over 0.9, outperforming other methods. RK-CCDs and UN-CCDs also perform well, with ARI values of 0.814 and 0.799, respectively. They detect 30 and 31 clusters, respectively, outperforming all other methods except KS-CCDs and K -means++.

Summary of the Experiment: Overall, KS-CCDs demonstrate the best performance, obtaining the highest Sil and competitive ARI values across almost all datasets. However, identifying the best density parameter δ for the KS-type statistic is computationally expensive. Even when the number of clusters is provided as an input parameter for K -means++ and spectral clustering, RK-CCDs and UN-CCDs maintain comparable performance, with UN-CCDs slightly better making them competitive clustering methods. DBSCAN and Louvain clustering methods yield slightly worse results than RK-CCDs. MST consistently produces negative ARI or Silhouette values, indicating the worst performance among the evaluated methods, since it is not robust to noise/outliers and the varying intensities of clusters.

6 Summary and Conclusion

In this paper, we propose a new CCD-based method for clustering, called UN-CCDs, which uses the NND instead of the Ripley’s K function to conduct the spatial randomness test.

UN-CCDs address the limitation of RK-CCDs in high-dimensional clustering, attributes to several enhancements discussed in Section 3.2. Through extensive Monte Carlo simulation in Section 4, we demonstrate that UN-CCDs are, in general, comparable to RK-CCDs in low-dimensional space, and deliver superior performance when the dimensionality $d \geq 10$. This is evidenced by the substantially higher Adjust Rand Index and the success rate in identifying the correct number of clusters. Moreover, as shown by the real and complex data analysis in Section 5, UN-CCDs maintain comparable performance to RK-CCDs and state-of-the-art methods such as spectral clustering and K -means++ (which require the number of clusters as an input parameter). These findings establish UN-CCDs as a robust and versatile clustering method, suitable for a wide range of data dimensionality and complexity. However, the UN-CCD method comes with some limitations: (1) It has high time complexity of $O(n^3)$. (2) It suffers reduced effectiveness in curtain in specific scenarios, e.g., when the dataset is consisted

of non-uniform clusters with low cluster intensities and close proximity. (3) The method currently requires manual tuning of the significance level (α) for its spatial randomness test.

Future Work: Lastly, we enumerate some interesting future work directions for UN-CCDs, including addressing the limitations of UN-CCDs and applying them to develop other clustering methods for different applications.

- (1) Extending UN-CCDs for Overlapping Clusters, developing methods similar to Fuzzy clustering.
- (2) Applying CCD-Based Clustering in Semi-Supervised Learning for partially labeled data.
- (3) Adaptive neighborhood or radius selection based on local density.
- (4) Developing automated process for tuning the significance levels (α) for the MC-SRT with NND, satisfying the need of different datasets.
- (5) The time complexity of the UN-CCD method is $O(n^3)$. Although it is faster than RK-CCDs, there is a substantial room for improvement.

7 Acknowledgements

Most of the Monte Carlo simulations in this paper were completed in part with the computing resource provided by the Auburn University Easley Cluster. The authors are grateful to Artür Manukyan for sharing the codes of KS-CCDs and RK-CCDs.

References

- [1] Rakesh Agrawal, Johannes Gehrke, Dimitrios Gunopulos, and Prabhakar Raghavan. Automatic subspace clustering of high dimensional data for data mining applications. In *Proceedings of the 1998 ACM SIGMOD International Conference on Management of Data*, pages 94–105, 1998.
- [2] Mihael Ankerst, Markus M Breunig, Hans-Peter Kriegel, and Jörg Sander. Optics: Ordering points to identify the clustering structure. *ACM Sigmod Record*, 28(2):49–60, 1999.
- [3] David Arthur and Sergei Vassilvitskii. k-means++: The advantages of careful seeding. Technical report, Stanford, 2006.
- [4] Adelchi Azzalini and Giovanna Menardi. Clustering via nonparametric density estimation: The r package pdfcluster. *ArXiv Preprint ArXiv:1301.6559*, 2013.
- [5] Julian Besag and Peter J Diggle. Simple monte carlo tests for spatial pattern. *Journal of the Royal Statistical Society Series C: Applied Statistics*, 26(3):327–333, 1977.
- [6] Kevin Beyer, Jonathan Goldstein, Raghu Ramakrishnan, and Uri Shaft. When is “nearest neighbor” meaningful? In *Database Theory—ICDT’99: 7th International Conference Jerusalem, Israel, January 10–12, 1999 Proceedings* 7, pages 217–235. Springer, 1999.
- [7] David M Blei, Andrew Y Ng, and Michael I Jordan. Latent dirichlet allocation. *Journal of Machine Learning Research*, 3(Jan):993–1022, 2003.
- [8] Vincent D Blondel, Jean-Loup Guillaume, Renaud Lambiotte, and Etienne Lefebvre. Fast unfolding of communities in large networks. *Journal of Statistical Mechanics: Theory and Experiment*, 2008(10):P10008, 2008.
- [9] Deyu Bo, Xiao Wang, Chuan Shi, Meiqi Zhu, Emiao Lu, and Peng Cui. Structural deep clustering network. In *Proceedings of the Web Conference 2020*, pages 1400–1410, 2020.
- [10] Vasek Chvatal. A greedy heuristic for the set-covering problem. *Mathematics of Operations Research*, 4(3):233–235, 1979.

- [11] Philip J Clark and Francis C Evans. Distance to nearest neighbor as a measure of spatial relationships in populations. *Ecology*, 35(4):445–453, 1954.
- [12] Philip J Clark and Francis C Evans. Generalization of a nearest neighbor measure of dispersion for use in k dimensions. *Ecology*, 60(2):316–317, 1979.
- [13] Dorin Comaniciu and Peter Meer. Mean shift: A robust approach toward feature space analysis. *IEEE Transactions on Pattern Analysis and Machine Intelligence*, 24(5):603–619, 2002.
- [14] Jason G DeVinney. *The class cover problem and its applications in pattern recognition*. PhD thesis, Johns Hopkins University, 2003.
- [15] Philip M Dixon, Abdel H El-Shaarawi, and Walter W Piegorsch. Ripley’s k function. *Encyclopedia of Environmetrics*, 3, 2012.
- [16] Harold Edson Driver and Alfred Louis Kroeber. *Quantitative expression of cultural relationships*, volume 31. Berkeley: University of California Press, 1932.
- [17] Dheeru Dua and Casey Graff. Uci machine learning repository, 2017.
- [18] Joseph C Dunn. A fuzzy relative of the isodata process and its use in detecting compact well-separated clusters. 1973.
- [19] Michael B Eisen, Paul T Spellman, Patrick O Brown, and David Botstein. Cluster analysis and display of genome-wide expression patterns. *Proceedings of the National Academy of Sciences*, 95(25):14863–14868, 1998.
- [20] Martin Ester, Hans-Peter Kriegel, Jörg Sander, and Xiaowei Xu. A density-based algorithm for discovering clusters in large spatial databases with noise. In *Proceedings of the Second International Conference on Knowledge Discovery and Data Mining (KDD-96)*, volume 96, pages 226–231, Portland, Oregon, USA, 1996. AAAI Press.
- [21] Absalom E Ezugwu, Abiodun M Ikotun, Olaide O Oyelade, Laith Abualigah, Jefery O Agushaka, Christopher I Eke, and Andronicus A Akinyelu. A comprehensive survey of clustering algorithms: State-of-the-art machine learning applications, taxonomy, challenges, and future research prospects. *Engineering Applications of Artificial Intelligence*, 110:104743, 2022.

- [22] Douglas H Fisher. Knowledge acquisition via incremental conceptual clustering. *Machine Learning*, 2:139–172, 1987.
- [23] Pasi Fränti and Sami Sieranoja. K-means properties on six clustering benchmark datasets, 2018.
- [24] Guojun Gan, Chaoqun Ma, and Jianhong Wu. *Data clustering: theory, algorithms, and applications*. Society for Industrial and Applied Mathematics, China, 2020.
- [25] James Gareth, Witten Daniela, Hastie Trevor, and Tibshirani Robert. *An introduction to statistical learning: with applications in R*. Springer, New York City, New York, 2013.
- [26] Michelle Girvan and Mark EJ Newman. Community structure in social and biological networks. *Proceedings of the National Academy of Sciences*, 99(12):7821–7826, 2002.
- [27] Sudipto Guha, Rajeev Rastogi, and Kyuseok Shim. Cure: An efficient clustering algorithm for large databases. *ACM Sigmod Record*, 27(2):73–84, 1998.
- [28] Sudipto Guha, Rajeev Rastogi, and Kyuseok Shim. Rock: A robust clustering algorithm for categorical attributes. *Information Systems*, 25(5):345–366, 2000.
- [29] Alexander Hinneburg, Daniel A Keim, et al. *An efficient approach to clustering in large multimedia databases with noise*, volume 98. Bibliothek der Universität, Konstanz, Germany, 1998.
- [30] Dorit S Hochbaum. Approximation algorithms for the set covering and vertex cover problems. *SIAM Journal on Computing*, 11(3):555–556, 1982.
- [31] Yaofang Hu and Wanjie Wang. Network-adjusted covariates for community detection. *Biometrika*, 111(4):1221–1240, 2024.
- [32] Lawrence Hubert and Phipps Arabie. Comparing partitions. *Journal of Classification*, 2:193–218, 1985.
- [33] Richard M Karp. Reducibility among combinatorial problems. In *Complexity of Computer Computations*, pages 85–103. Springer, 1972.
- [34] George Karypis, Eui-Hong Han, and Vipin Kumar. Chameleon: Hierarchical clustering using dynamic modeling. *Computer*, 32(8):68–75, 1999.

- [35] Leonard Kaufman and Peter J Rousseeuw. *Finding groups in data: an introduction to cluster analysis*. John Wiley & Sons, 2009.
- [36] Raghuram Krishnapuram and James M Keller. The possibilistic c-means algorithm: insights and recommendations. *IEEE Transactions on Fuzzy Systems*, 4(3):385–393, 1996.
- [37] James MacQueen. Classification and analysis of multivariate observations. In *5th Berkeley Symp. Math. Statist. Probability*, pages 281–297, 1967.
- [38] Artür Manukyan and Elvan Ceyhan. Classification of imbalanced data with a geometric digraph family. *The Journal of Machine Learning Research*, 17(1):6504–6543, 2016.
- [39] Artür Manukyan and Elvan Ceyhan. Parameter free clustering with cluster catch digraphs (technical report). *ArXiv Preprint ArXiv:1912.11926*, 2019.
- [40] David J Marchette. *Random graphs for statistical pattern recognition*. John Wiley & Sons, Hoboken, New Jersey, 2005.
- [41] Glenn W Milligan and Martha C Cooper. An examination of procedures for determining the number of clusters in a data set. *Psychometrika*, 50:159–179, 1985.
- [42] Andrew Ng, Michael Jordan, and Yair Weiss. On spectral clustering: Analysis and an algorithm. *Advances in neural information processing systems*, 14, 2001.
- [43] Raymond T Ng and Jiawei Han. Clarans: A method for clustering objects for spatial data mining. *IEEE Transactions on Knowledge and Data Engineering*, 14(5):1003–1016, 2002.
- [44] Nikhil R Pal, Kuhu Pal, James M Keller, and James C Bezdek. A possibilistic fuzzy c-means clustering algorithm. *IEEE Transactions on Fuzzy Systems*, 13(4):517–530, 2005.
- [45] Carey E Priebe, David J Marchette, Diego Socolinsky, and Jason DeVinney. Classification using class cover catch digraphs. *Journal of Classification*, 20:3–23, 2003.
- [46] Lawrence Rabiner and Biinghwang Juang. An introduction to hidden markov models. *IEEE Assp Magazine*, 3(1):4–16, 1986.

[47] Xingcheng Ran, Yue Xi, Yonggang Lu, Xiangwen Wang, and Zhenyu Lu. Comprehensive survey on hierarchical clustering algorithms and the recent developments. *Artificial Intelligence Review*, 56(8):8219–8264, 2023.

[48] Carl Rasmussen. The infinite gaussian mixture model. *Advances in Neural Information Processing Systems*, 12, 1999.

[49] Mohammad Rezaei and Pasi Fränti. Can the number of clusters be determined by external indices? *IEEE Access*, 8:89239–89257, 2020.

[50] Brian D Ripley. The second-order analysis of stationary point processes. *Journal of Applied Probability*, 13(2):255–266, 1976.

[51] Peter J Rousseeuw. Silhouettes: a graphical aid to the interpretation and validation of cluster analysis. *Journal of Computational and Applied Mathematics*, 20:53–65, 1987.

[52] Amit Saxena, Mukesh Prasad, Akshansh Gupta, Neha Bharill, Om Prakash Patel, Aruna Tiwari, Meng Joo Er, Weiping Ding, and Chin-Teng Lin. A review of clustering techniques and developments. *Neurocomputing*, 267:664–681, 2017.

[53] Erich Schubert, Jörg Sander, Martin Ester, Hans Peter Kriegel, and Xiaowei Xu. Dbscan revisited, revisited: why and how you should (still) use dbscan. *ACM Transactions on Database Systems (TODS)*, 42(3):1–21, 2017.

[54] Gholamhosein Sheikholeslami, Surojit Chatterjee, and Aidong Zhang. Wavecluster: a wavelet-based clustering approach for spatial data in very large databases. *The VLDB Journal*, 8(3):289–304, 2000.

[55] Luyi Shen, Arash Amini, Nathaniel Josephs, and Lizhen Lin. Bayesian community detection for networks with covariates. *Bayesian Analysis*, 20(3):735–762, 2025.

[56] Rui Shi, Nedret Billor, and Elvan Ceyhan. Outlier detection with cluster catch digraphs. *arXiv preprint arXiv:2409.11596*, 2024.

[57] Rui Shi, Nedret Billor, and Elvan Ceyhan. Outlyingness scores with cluster catch digraphs. *arXiv preprint arXiv:2501.05530*, 2025.

[58] Thorvald Sørensen. A method of establishing groups of equal amplitude in plant sociology based on similarity of species content and its application to analyses of the vegetation on danish commons. *Biologiske Skrifter*, 5:1–34, 1948.

[59] Prateek R Srivastava, Purnamrita Sarkar, and Grani A Hanususanto. A robust spectral clustering algorithm for sub-gaussian mixture models with outliers. *Operations Research*, 71(1):224–244, 2023.

[60] Vincent A Traag, Ludo Waltman, and Nees Jan Van Eck. From louvain to leiden: guaranteeing well-connected communities. *Scientific Reports*, 9(1):1–12, 2019.

[61] Cor J. Veenman, Marcel J. T. Reinders, and Eric Backer. A maximum variance cluster algorithm. *IEEE Transactions on Pattern Analysis and Machine Intelligence*, 24(9):1273–1280, 2002.

[62] Juha Vesanto and Esa Alhoniemi. Clustering of the self-organizing map. *IEEE Transactions on Neural Networks*, 11(3):586–600, 2000.

[63] Hongzhi Wang, Mohamed Jaward Bah, and Mohamed Hammad. Progress in outlier detection techniques: A survey. *IEEE Access*, 7:107964–108000, 2019.

[64] Wei Wang, Jiong Yang, Richard Muntz, et al. Sting: A statistical information grid approach to spatial data mining. In *Vldb*, volume 97, pages 186–195. Citeseer, 1997.

[65] Joe H Ward Jr. Hierarchical grouping to optimize an objective function. *Journal of the American Statistical Association*, 58(301):236–244, 1963.

[66] Michel Wedel and Wagner A Kamakura. *Market segmentation: Conceptual and methodological foundations*. Springer Science & Business Media, 2000.

[67] Daniela Witten and Gareth James. *An introduction to statistical learning with applications in R*. Springer Publication, New York City, New York, 2013.

[68] Xiaowei Xu, Martin Ester, Hans-Peter Kriegel, and Jörg Sander. A distribution-based clustering algorithm for mining in large spatial databases. In *Proceedings 14th International Conference on Data Engineering*, pages 324–331. IEEE, 1998.

[69] Hui Yin, Amir Aryani, Stephen Petrie, Aishwarya Nambissan, Aland Astudillo, and Shengyuan Cao. A rapid review of clustering algorithms. *ArXiv Preprint ArXiv:2401.07389*, 2024.

[70] Charles T Zahn. Graph-theoretical methods for detecting and describing gestalt clusters. *IEEE Transactions on Computers*, 100(1):68–86, 1971.

- [71] Dao-Qiang Zhang and Song-Can Chen. A novel kernelized fuzzy c-means algorithm with application in medical image segmentation. *Artificial Intelligence in Medicine*, 32(1):37–50, 2004.
- [72] Ji Zhang. Advancements of outlier detection: A survey. *ICST Transactions on Scalable Information Systems*, 13(1):1–26, 2013.
- [73] Ji Zhang, Wynne Hsu, and Mong Li Lee. Clustering in dynamic spatial databases. *Journal of Intelligent Information Systems*, 24(1):5–27, 2005.
- [74] Tian Zhang, Raghu Ramakrishnan, and Miron Livny. Birch: an efficient data clustering method for very large databases. *ACM Sigmod Record*, 25(2):103–114, 1996.